Impact of energy-momentum nonconservation
on radial pulsations of strange stars

H. Maulana and A. Sulaksono

Departemen Fisika, Fakultas Matematika dan Ilmu Pengetahuan Alam,
Universitas Indonesia, Depok 16424, Indonesia

We use ideal fluid energy conditions to constrain the free parameter of the degree of nonconservation ζ of the energy-momentum tensor in Rastall gravity theory. We study the mass-radius relation of strange stars and the corresponding stability using the obtained range of ζ constrained by energy conditions. In our calculations, we use the MIT bag model with a color-flavor-locked state to describe strange quark matter. We obtain a finite, narrow range of $0 \leq \zeta \leq 0.5$. In addition to ζ, the corresponding nonconservation of the energy-momentum tensor depends on the gradient of the energy-momentum scalar. The behavior of matter in the MIT bag model is one example in which the energy-momentum tensor is conserved through the zero value on the gradient of the energy-momentum scalar. We also find that the corresponding mass-radius relation of strange stars depends on the interplay of matter parameters, such as m_s, B, Δ, and the Rastall parameter ζ. In addition, we find that as ζ increases, the maximum strange star mass decreases. Furthermore, the stability of strange stars with regard to radial oscillations in Rastall gravity theory is rather different from that in general relativity because of the impact of the nonconservation of the energy-momentum tensor. The stability boundary mass and radius determined from the zero modes of radial perturbation oscillations are not the same as the maximum mass and corresponding radius. This is because the Rastall nonconservation term increases the matter pressure to support the strange star against collapse, especially when $v_s^2 > 1/3$. The reverse applies when $v_s^2 < 1/3$.

I. INTRODUCTION

General relativity (GR) is a pillar of contemporary physics. GR passes almost all observational tests at intermediate energy scales. With the introduction of concepts such as dark matter (DM) and dark energy (DE), GR has also passed tests at higher energy scales. However, GR is a classical theory, so for phenomena at high energy scales it could yield a singularity that can only be resolved by including quantum corrections. Furthermore, firm experimental evidence of the existence of DM and DE is still lacking. These issues motivate the study of alternative or modified gravity theories (e.g., Refs. [1–3]). Alternative or modified gravity theories can be categorized into those that obey or disobey energy-momentum conservation [4–10]. Nonconservation of the energy-momentum tensor is also found in relativistic diffusion models (Ref. [11] and references therein). Note also that the nonconservation of energy-momentum is phenomenologically confirmed by the physical particle creation process in cosmology (Ref. [12] and references therein). Rastall gravity theory [4] can be considered a phenomenological extension of GR with the simplest form of the energy-momentum nonconservation equation, in which the covariant divergence of the energy-momentum tensor is proportional to the Ricci

scalar. Therefore, when the geometry is flat, energy-momentum is still conserved. This feature can be considered the phenomenological consequence of the appearance of quantum fluctuation corrections in curved space-time within a classical framework [13,14]. Rastall gravity theory has a relatively richer structure than GR and could yield different and novel behavior for compact objects such as neutron stars [15] or strange stars (SSs). For such compact objects, however, a systematic study of permissible parameter values and a stability analysis of Rastall gravity remains lacking. Furthermore, the applications of Rastall gravity to SSs have not been systematically studied. On the other hand, we note recent intense discussion on the equivalence of Rastall and GR theories [16–18].

The potential existence of SSs is a consequence of the idea that the presence of strange quarks can lower the binding energy of strange quark matter (SQM) in weak equilibrium below that of ^{56}Fe (absolute stability of quark matter). The MIT bag model provides the simplest description of absolutely stable SQM. In that model, the quarks are free, with confinement provided through a bag constant. We note, however, that the attractive force among quarks that are antisymmetric in color tends to pair quarks that are close to the Fermi surface at high densities. It has recently been shown that a color-flavor-locked (CFL) state, in which

quarks near the Fermi surface form pairs, seems to be more energetically favorable and widens the stability window [19] (see also Ref. [20] and references therein). A recent review of the role of color superconductivity in dense quark matter can be found in Ref. [21]. It is also worth pointing out that a detailed analysis of pulsar timing data in pulsar evolution has shown that the SQM model is consistent with both radio and x-ray observations, whereas the ordinary nuclear matter model requires enhancement by a dumping mechanism [22]. CFL SQM can also potentially be found in the inner cores of neutron stars (hybrid stars) [23].

Within a GR framework, stellar oscillations were studied for the first time by Chandrasekhar [24] in 1964. These stellar oscillation studies still attract much interest now because of their potential to reveal key information about the inner structure of compact objects and shed light on the equation of state (EoS) of the corresponding dense matter (Ref. [25] and references therein). Several studies on the radial oscillation of SQM and hybrid stars have also been reported (Refs. [25–28] and references therein). However, a radial oscillation analysis of SQM within a Rastall gravity framework has not yet been explored. Keeping that theory in mind, the corresponding energy-momentum for the MIT bag model with a speed of sound $v_s = 1/\sqrt{3}$ is still conserved in a Rastall framework, and the MIT bag model with SQM described by a CFL state is preferable for the proper exploration of the impact of energy-momentum nonconservation on stability.

In this work, we systematically investigate the allowed free parameter values of Rastall gravity theory using several well-known energy conditions. We further investigate the impacts of the corresponding free parameter value on SS static properties such as mass and radius. We use radial pulsation analysis to test the stability of CFL SQM for SSs in a Rastall gravity framework.

This paper is organized as follows. In Sec. II we review the Rastall gravity theory in general, and discuss the possibility of constraining Rastall free parameter values using several energy conditions. In Sec. III we briefly discuss the EoS of CFL SQM in SSs. In Sec. IV we discuss the bulk properties and radial pulsations of SSs within Rastall gravity theory. Finally, the conclusions are given in Sec. V.

II. RASTALL GRAVITY THEORY

The field equation of Rastall gravity theory is [15]

$$G_{\mu\nu} - \gamma g_{\mu\nu} R \equiv 8\pi G T_{\mu\nu}, \tag{1}$$

where $\gamma = (\eta - 1)/2$ and η denotes the Rastall free parameter. Note that if the parameter η is set to 1, the field equation reverts to that of GR. The divergence of the energy-momentum tensor of Rastall theory obeys the following relation:

$$T^{\mu}_{\nu;\mu} = \zeta T_{;\nu}, \tag{2}$$

where

$$\zeta = \frac{1}{2}\left(\frac{\eta - 1}{2\eta - 1}\right). \tag{3}$$

ζ indicates the degree of nonconservation of the energy-momentum tensor. In the case of spherically symmetric stars with an isotropic ideal fluid EoS, only the radial component of $T^{\mu}_{\nu;\mu}$ exists. Therefore, we can write $T^{\mu}_{1;\mu}$ as

$$T^{\mu}_{1;\mu} = \zeta \frac{dT}{dr} = \zeta\left(3 - \frac{d\rho}{dp}\right)\frac{dp}{dr}. \tag{4}$$

It can be seen from Eq. (4) that the conservation of energy-momentum is fulfilled not only for $\eta = 1$, but also for $\frac{dT}{dr} = 0$ or $\frac{d\rho}{dp} = 3$, though the latter is exactly obeyed for an EoS of the MIT bag model with a speed of sound $v_s = \frac{1}{\sqrt{3}}$. We will show later that, besides the value of ζ, the nonzero value of $T^{\mu}_{1;\mu}$ due to $\frac{dT}{dr}$ also affects SS stability.

Several studies have attempted to construct Rastall gravity theory from the Einstein-Hilbert Lagrangian [8,13,29]. However, the proper form of the Lagrangian density for Rastall gravity has yet to be determined. Dzhunushaliev and Quevedo [13] tried to relate Rastall gravity theory with quantum fluctuations of the space-time of the corresponding volume elements. They started from the Einstein-Hilbert Lagrangian and incorporated the fluctuation factor into the variation of $\sqrt{-g}$. The corresponding fluctuation factor was treated like the Rastall parameter. As a result, they found a field equation similar to that of Rastall gravity, but with a fluctuating factor in the energy-momentum tensor instead of in the Einstein tensor field. As de Santos and Nogales [8] pointed out, Rastall gravity theory can be considered a particular case of $f(R,T)$ theory, where $f(R,T)$ is constructed from the corresponding Lagrangian density. However, in this work we do not focus on this perspective.

Here we are concerned more with how to constrain the value of free parameter of the Rastall ζ using fundamental bases such as energy conditions. Below, we investigate the range of the ζ value by transforming Rastall gravity theory using an isotropic ideal fluid EoS into a GR-like framework with an apparent EoS. We can check the compatibility of the corresponding apparent EoS with GR energy conditions. The energy conditions are the criteria for the physically admissible energy-momentum tensor of matter in GR. These criteria are sufficiently strong to rule out the nonphysical solution of the Einstein field equations; the ideas that energy has a positive value and that gravity is attractive are also already encoded in these criteria.

We start by rewriting Eq. (1) in the from of a GR effective field equation as follows [15]:

$$G_{\mu\nu} = 8\pi G \tilde{T}_{\mu\nu}, \tag{5}$$

where the effective (apparent) energy-momentum tensor $\tilde{T}_{\mu\nu}$ is

$$\tilde{T}_{\mu\nu} = T_{\mu\nu} - \frac{1}{2}\left(\frac{\eta-1}{2\eta-1}\right)g_{\mu\nu}T. \tag{6}$$

We can also express $\tilde{T}_{\mu\nu}$ as the usual energy-momentum tensor for an isotropic ideal fluid by defining the apparent pressure $\tilde{p}$ and density $\tilde{\rho}$, which depend on parameter η as follows:

$$\tilde{p} = \frac{1}{2}\left(\frac{\eta-1}{2\eta-1}\right)\rho + \frac{1}{2}\left(\frac{\eta+1}{2\eta-1}\right)p, \tag{7}$$

$$\tilde{\rho} = \frac{1}{2}\left(\frac{3\eta-1}{2\eta-1}\right)\rho + \frac{1}{2}\left(\frac{3\eta-3}{2\eta-1}\right)p. \tag{8}$$

It is clear that $\tilde{p}$ and $\tilde{\rho}$ are singular for $\eta = 1/2$. Below, we study the compatibility of the apparent EoS of Rastall gravity [Eqs. (7)–(8)] with various energy conditions:

(1) Null energy condition (NEC): $\tilde{T}_{\mu\nu}l^{\mu}l^{\nu} \geq 0$, where l^{μ} is a null vector in which $g_{\mu\nu}l^{\mu}l^{\nu} = 0$ is satisfied. This condition is equivalent to the condition that $\tilde{p} + \tilde{\rho} \geq 0$. This condition cannot limit the Rastall parameter because $\tilde{p} + \tilde{\rho} = p + \rho$.

(2) Weak energy condition (WEC): $\tilde{T}_{\mu\nu}t^{\mu}t^{\nu} \geq 0$, where t^{μ} is a timelike vector in which $g_{\mu\nu}t^{\mu}t^{\nu} \leq 0$ is satisfied. This condition is equivalent to the conditions that $\tilde{p} + \tilde{\rho} \geq 0$ and $\tilde{\rho} \geq 0$. Because we assume that the magnitude of the density ρ is positive, we can safely divide the corresponding inequality by the ρ of an ideal fluid, and if we define the EoS parameter $w \equiv \frac{p}{\rho}$ the inequality becomes

$$\frac{1}{2}\left(\frac{3\eta-1}{2\eta-1}\right) + \frac{1}{2}\left(\frac{3\eta-3}{2\eta-1}\right)w \geq 0. \tag{9}$$

For some specific w values, Eq. (9) can be expressed as

$$\left\{\eta > \frac{1}{2}\right\} \quad \text{for } w = -1,$$

$$\left\{\eta \leq \frac{1+3w}{3+3w} \cup \eta > \frac{1}{2}\right\} \quad \text{for } -1 < w < \frac{1}{3},$$

$$\left\{\eta < \frac{1}{2} \cup \eta > \frac{1}{2}\right\} \quad \text{for } w = \frac{1}{3},$$

$$\left\{\eta < \frac{1}{2} \cup \eta \geq \frac{1+3w}{3+3w}\right\} \quad \text{for } w > \frac{1}{3}. \tag{10}$$

The inequalities in Eq. (9) are shown in Fig. 1. The shaded areas in Fig. 1 indicate the regions allowed by the WEC. The blue area is for stellar matter with $w \geq 0$
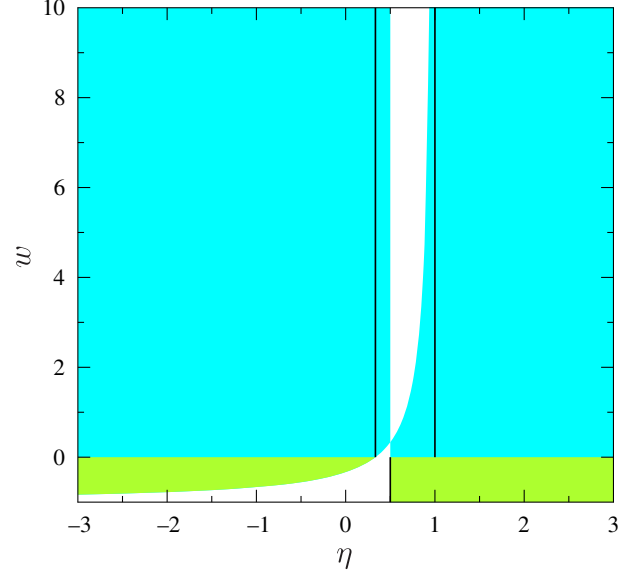

FIG. 1. Fulfillment of the WEC. The weak energy condition is represented by the shaded regions of the EoS parameter w as a function of the Rastall free parameter η. For $w \geq 0$ (blue area), the black vertical line $\eta = 1/3$ indicates a boundary such that the area on the left-hand side of this line fully satisfies the WEC, and the black vertical line $\eta = 1$ indicates the boundary such that the area on the right-hand side of the line fully satisfies the WEC. For $-1 \leq w < 0$ (green area), the black vertical line $\eta = 0.5$ indicates the boundary such that the area on the right-hand side of the line fully satisfies the WEC. Although it is not shown in the figure, note that in the limit $\eta = \pm\infty$, $w = -1$.

and the green area is for dark energy EoS with $-1 \leq w < 0$. Note that, in general, the actual w value for a specific EoS is not constant, but rather depends on the density of the EoS. Therefore, the allowed values of the parameter η according to the energy conditions also vary with density. However, all w values predicted by acceptable EoSs are still within these ranges. For positive w values, by taking w equal to infinity as the upper limit and w equal to zero as the lower limit, we find that the blue shaded areas safely satisfy the WEC for $\eta \leq \frac{1}{3}$ and $\eta \geq 1$. On the other hand, in cosmology, we might deal with negative pressure or with negative w. In such cases, $-1 \leq w < 0$, the green shaded area safely satisfies the WEC for $\eta \geq 1/2$.

(3) Strong energy condition (SEC): $\tilde{T}_{\mu\nu}t^{\mu}t^{\nu} \geq \frac{1}{2}\tilde{T}_{\lambda}^{\lambda}t^{\sigma}t_{\sigma}$. This condition is equivalent to $\tilde{\rho} + \tilde{p} \geq 0$ and $\tilde{\rho} + 3\tilde{p} \geq 0$, respectively. By using the same procedure as that of the NEC and WEC, we can arrive at the following inequality:

$$\left(\frac{3\eta-2}{2\eta-1}\right) + \left(\frac{3\eta}{2\eta-1}\right)w \geq 0, \tag{11}$$

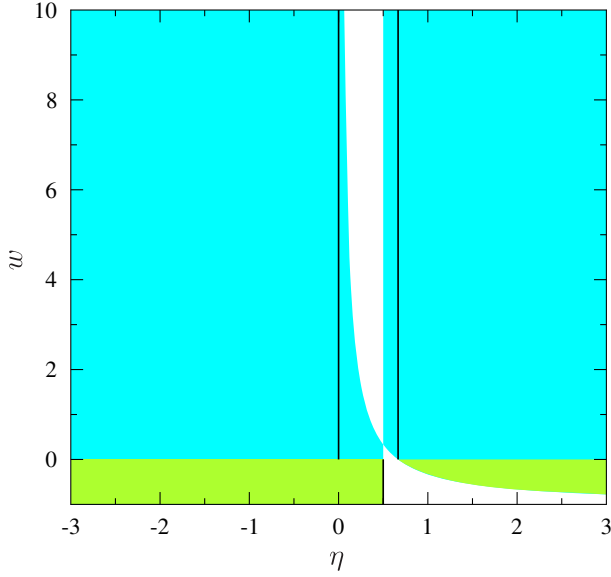where for some specific values of w, Eq. (11) can be expressed as

FIG. 2. The fulfillment of the SEC. The strong energy condition is represented by the shaded regions of the EoS parameter w as a function of the Rastall parameter η. For $w \geq 0$ (blue area), the black vertical line $\eta = 0$ indicates a boundary such that the area on the left-hand side of this line fully satisfies the SEC, and the black vertical line $\eta = 2/3$ indicates the boundary such that the area on the right-hand side of the line fully satisfies the SEC. For $-1 \leq w < 0$ (green area), the black vertical line $\eta = 0.5$ indicates the boundary such that the area on the right-hand side of the line fully satisfies the SEC. Although it is not shown in the figure, note that in the limit $\eta = \pm\infty$, $w = -1$.

$$\left\{ \eta < \frac{1}{2} \right\} \quad \text{for } w = -1,$$

$$\left\{ \eta < \frac{1}{2} \cup \eta \geq \frac{2}{3 + 3w} \right\} \quad \text{for } -1 < w < \frac{1}{3},$$

$$\left\{ \eta < \frac{1}{2} \cup \eta > \frac{1}{2} \right\} \quad \text{for } w = \frac{1}{3},$$

$$\left\{ \eta \leq \frac{2}{3 + 3w} \cup \eta > \frac{1}{2} \right\} \quad \text{for } w > \frac{1}{3}. \quad (12)$$

The SEC inequalities are shown in Fig. 2. In general, the shaded areas in Fig. 2 indicate the values allowed by the SEC. For positive w, by taking the same upper and lower limits of w as for the WEC above, we find that the blue shaded areas safely satisfy the SEC for $\eta \geq \frac{2}{3}$ and $\eta \leq 0$. The constraint on η from the SEC is different than that from the WEC. However, there is an overlap in the corresponding shaded areas, be the one with blue or the one with green color of the WEC and that of the SEC. For $w \geq 0$, the corresponding overlapping shaded area is safely restricted by $\eta \leq 0$ and $\eta \geq 1$. On the other hand, for $-1 \leq w < 0$, the corresponding overlapping shaded area is restricted by $\eta < 1/2$. We can conclude that,

for the full range $-1 \leq w < 0$, the combination of WEC and SEC requirements is fully satisfied only by $\eta = \pm\infty$ which is related to $\zeta = 0.25$. Of course, it is still possible to find values of η in between $\eta = +\infty$ and $\eta = -\infty$ for a constant w between $-1 < w < 0$ that are compatible with both energy conditions. However, this is not the case for all values of η in $-1 < w < 0$.

(4) Dominant energy condition (DEC): $\tilde{T}_{\mu\nu}t^\mu t^\nu \geq 0$ and $\tilde{T}_{\mu\nu}\tilde{T}^\nu_\lambda t^\mu t^\lambda \leq 0$. The DEC is equivalent to $\tilde{\rho} \geq 0$ and $\tilde{\rho} \pm \tilde{p} \geq 0$, respectively. We find that the inequality becomes

$$\left(\frac{\eta}{2\eta - 1} \right) + \left(\frac{\eta - 2}{2\eta - 1} \right) w \geq 0, \quad (13)$$

and for some specific w values, together with (9), Eq. (13) can be reduced to the following inequalities:

$$\left\{ \eta > \frac{1}{2} \right\} \quad \text{for } w = -1,$$

$$\left\{ \eta \leq \frac{2w}{1 + w} \cup \eta > \frac{1}{2} \right\} \quad \text{for } -1 < w < \frac{1}{3},$$

$$\left\{ \eta < \frac{1}{2} \cup \eta > \frac{1}{2} \right\} \quad \text{for } w = \frac{1}{3},$$

$$\left\{ \eta < \frac{1}{2} \cup \eta \geq \frac{2w}{1 + w} \right\} \quad \text{for } \frac{1}{3} < w \leq 1. \quad (14)$$

The DEC inequalities are shown in Fig. 3. However, for the DEC, the allowed w values are restricted to the range $-1 \leq w \leq 1$. For positive w values in this range, by taking the upper and lower limits of w from this range, we find that the blue shaded areas to the right and left of the vertical black lines $\eta = 1$ and $\eta = 0$, respectively, satisfy the DEC. For negative w values in this range, the green shaded area safely satisfies the DEC on the right-hand side of $\eta = 1/2$. By comparing this result with those from the NEC, WEC, and SEC requirements, the range of η based on the DEC is more restrictive and the corresponding range of η also satisfies the other energy conditions.

Therefore, we will use the allowed DEC η range result as the range of the parameter η accepted by all energy conditions. It seems that these energy conditions allow a rather wide range for the Rastall free parameter η. However, if we translate the corresponding η range into the range of ζ, we obtain a finite, narrow range of $0 \leq \zeta \leq 0.5$. Therefore, from this point forward, we prefer to use ζ as a free parameter which is, in general, always valid for stellar matter. We further take ζ values of 0, 0.125, 0.25, 0.375, and 0.5 as representative of the allowed free parameter values for Rastall gravity.

It is worth noting that energy conditions in some modified gravity theories focusing on cosmology applications have
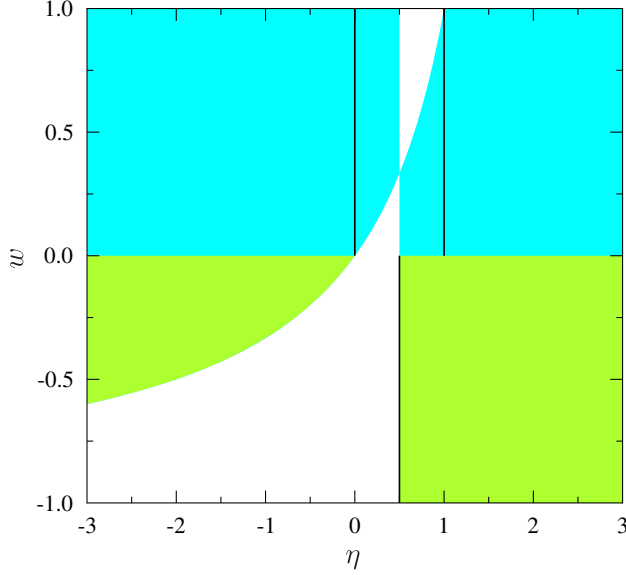
FIG. 3. The DEC. The dominant energy condition is represented by the shaded regions of the EoS parameter w as a function of the Rastall parameter η. For $1 \leq w \leq 0$ (blue area), the black vertical line $\eta = 0$ indicates a boundary such that the area on the left-hand side of this line fully satisfies the DEC, and the black vertical line $\eta = 1$ indicates the boundary such that the area on the right-hand side of the line fully satisfies the DEC. For $-1 \leq w < 0$ (green area), the black vertical line $\eta = 0.5$ indicates the boundary such that the area on the right-hand side of this line fully satisfies the DEC. Although it is not shown in the figure, note that in the limit $\eta = \pm\infty$, $w = -1$.

been studied (e.g., Refs. [30–32]). Moradpour and Salako [33] studied the thermodynamics of static spherically symmetric field equations within Rastall theory. In accordance with the horizon entropy positivity requirement, they found that this constraint is compatible with $\zeta > -0.5$ ($\eta < 1/2$ and $\eta > 2/3$). Our range result is more restricted but quite compatible with that of Moradpour and Salako [33]. Observational constraints on Rastall cosmology were explored in Refs. [34,35]. They found that, according to Bayesian analysis, the Rastall parameter ζ cannot be strictly constrained and the observational data cluster around a w value of -1. They also showed that evolution from small perturbations is unstable if $w \neq -1$ and $\zeta \neq 0$. Furthermore, they found that, for matter described by a two-fluid model (with one component representing vacuum energy and the other pressureless matter), the cosmological scenario of Rastall theory is the same as that of the ΛCDM model. Our results show that the energy conditions yield unnatural η values in the case of $w = -1$. On the other hand, Batista *et al.* [34,35] reported that they could not constrain the ζ parameter for $w = -1$. Interestingly, Oliveira *et al.* [36] found that there are two vacuum solutions for Rastall gravity, namely, the Schwarzchild metric solution for $\eta \neq 1/2$ and the Schwarzchild–de Sitter metric solution for $\eta = 1/2$. The appearance of an integration constant (cf. cosmological constant) for the $1/2$ case allows Rastall gravity to be

considered as unimodular gravity [37]. Hansraj *et al.* [18] studied the solution of a Tolman metric model within Rastall theory. They found that for $\eta = 1/2$, Rastall theory successfully fulfills all physical requirements for Tolman models. The latter results are in stark contrast to the singularity $T^{\mu}_{\nu;\mu}$ when $\eta = 1/2$.

III. EQUATION OF STATE OF STRANGE STARS

Here we briefly discuss SQM based on the MIT bag model with a CFL state. The SQM is composed of u, d, and s quarks and no electrons, making the SQM electrically neutral. The CFL phase involves pairing interaction, which is relates to the formation of ud, us, and ds Cooper pairs. The corresponding MIT bag $+$ CFL state model thermodynamic potential of order Δ^2 is given by [19,23]

$$\Omega_{\text{CFL}} = \Omega_{\text{free}} - \frac{3\Delta^2\mu^2}{\pi^2} + B, \tag{15}$$

with

$$\Omega_{\text{free}} = \frac{6}{\pi^2} \int_0^\nu p_f^2(p_f - \mu)dp_f + \frac{3}{\pi^2} \int_0^\nu p_f^2\left(\sqrt{p_f^2 + m_s^2} - \mu\right)dp_f, \tag{16}$$

where Ω_{free} is the thermodynamic potential for free quarks without pairing interaction and μ is the baryon chemical potential, i.e., $\mu = (\mu_u + \mu_d + \mu_s)/3$. The pairing interaction forces the flavors to have the same Fermi momentum and number density. In this case, the Fermi momentum of the SQM is given by

$$\nu = 2\mu - \sqrt{\mu^2 + \frac{m_s^2}{3}}. \tag{17}$$

The term $3\Delta^2\mu^2/\pi^2$ is called the condensate term and Δ is the pairing gap [19]. B is the bag constant, which is related to physical confinement.

We write the pressure and energy density of the corresponding SQM in their standard form as follows:

$$p = -\Omega_{\text{CFL}}, \tag{18}$$

$$\rho = 3\mu n_B - p, \tag{19}$$

where the baryon number density is defined as

$$n_B = n_u = n_d = n_s = \frac{(\nu^3 + 2\Delta^2\mu)}{\pi^2}. \tag{20}$$

To simplify the calculations, we assume m_s to be relatively small compared to μ. This approximation is expected to be accurate at high density. From the above equations, we can write the EoS as

$$\rho = 3p + 4B - \frac{9\alpha\mu^2}{\pi^2}, \tag{21}$$

where μ^2 and α are

$$\mu^2 = -3\alpha + \left[\frac{4}{3}\pi^2(B+p) + 9\alpha^2\right]^{1/2}, \tag{22}$$

$$\alpha = -\frac{m_s^2}{6} + \frac{2\Delta^2}{3}. \tag{23}$$

We can easily obtain $d\rho/dp$ from Eq. (21) as

$$\frac{d\rho}{dp} = \frac{3(\mu^2 + \alpha)}{\mu^2 + 3\alpha}. \tag{24}$$

The explicit form of $d\rho/dp$ is needed to calculate the effective adiabatic index used in the stability analysis. From Eqs. (21)–(22), we can also obtain the relation

$$p = \frac{\rho}{3} - \frac{4B}{3} + \frac{3\alpha\mu^2}{\pi^2}, \tag{25}$$

with μ^2 now expressed as

$$\mu^2 = -\alpha + \left[\alpha^2 + \frac{4}{9}\pi^2(\rho - B)\right]^{1/2}. \tag{26}$$

The actual values of B, m_s, and Δ are not accurately known. Therefore, they can be considered free parameters and can be constrained by the stability conditions [38,39]. The first condition is that the energy per baryon must be smaller than the neutron mass at zero pressure and temperature. From this condition, we have [38,39]

$$3\mu \leq m_n. \tag{27}$$

If we evaluate Eq. (22) at zero pressure, we can define $m_s - B$ using the following inequality:

$$B < -\frac{m_s^2 m_n^2}{12\pi^2} + \frac{\Delta^2 m_n^2}{3\pi^2} + \frac{m_n^4}{108\pi^2}. \tag{28}$$

The second condition is that the magnitude of the bag constant must be greater than 57 MeV [39]. The stability windows of SQM can be related to both conditions [38]. Figure 4 shows the SQM EoSs for some ranges of Δ, B, and m_s variation. In general, the SQM EoS based on the MIT bag model with a CFL state depends on the interplay of the parameters m_s, B, and Δ. The SQM pressure increases almost linearly with increasing density and increasing m_s, whereas decreasing B values make the SQM EoS stiffer such that, for a fixed density, the pressure is higher. These results can be understood from Eqs. (25)–(26). The increased SQM pressure for a fixed density is mostly due to the effect of B and is enhanced by both m_s
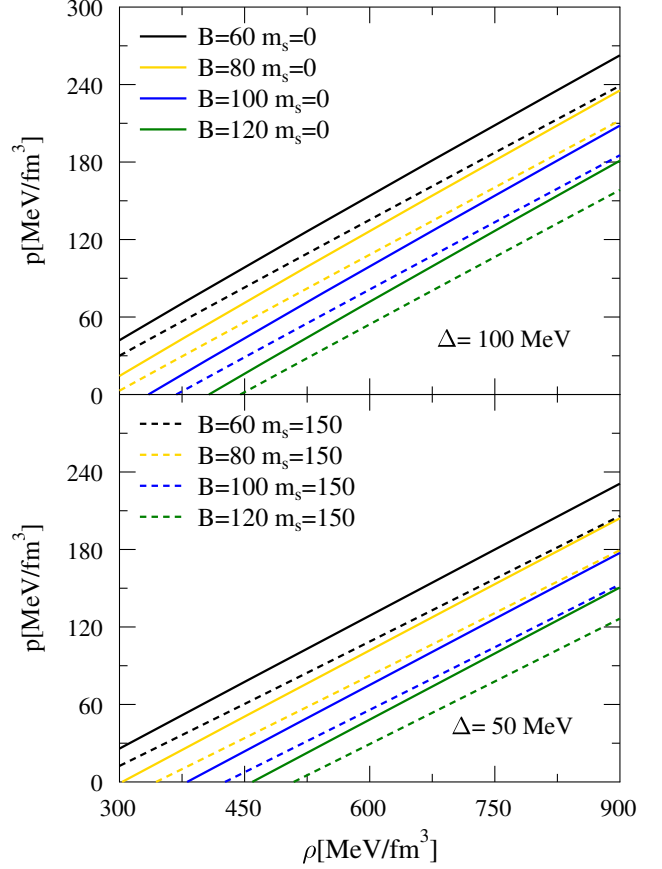

FIG. 4. The pressure p as a function of density ρ for various values of B and m_s. The solid and dashed lines represent $m_s = 0$ and $m_s = 150$, respectively. The various values of B are denoted by the colored lines. The upper and lower panels are for $\Delta = 100$ and $\Delta = 50$, respectively.

and Δ, and the slope of the SQM EoS is dominated by the factor $1/3$ and enhanced by the contribution of m_s as well as that of μ^2.

IV. RADIAL PULSATIONS IN RASTALL GRAVITY

Here we briefly discuss the SQM instability due to radial pulsations in Rastall gravity theory. The SQM can be considered as an isotropic ideal fluid. The actual energy-momentum tensor takes the form

$$T_{\mu\nu} = pg_{\mu\nu} + (\rho + p)u_\mu u_\nu, \tag{29}$$

and the spherically symmetric and static metric of SSs reads as follows:

$$ds^2 = -e^\nu dt^2 + e^\lambda dr^2 + r^2 d\theta^2 + r^2 \sin^2\theta d\phi^2. \tag{30}$$

Given the energy-momentum tensor (29) and the metric (30), the Einstein field equations can be easily integrated to give hydrostatic equilibrium equations known as Tolman-Oppenheimer-Volkoff (TOV) equations. To find the TOV equations in Rastall gravity theory, we adopt the same

procedure to obtain the corresponding hydrostatic equilibrium equations of GR. The corresponding equations can be written as [15]

$$\frac{d\tilde{p}}{dr} = -\frac{G}{r^2}\frac{(\tilde{\rho} + \tilde{p})(\tilde{M} + 4\pi r^3 \tilde{p})}{1 - \frac{2G\tilde{M}}{r}}, \qquad (31)$$

$$\frac{d\tilde{M}}{dr} = 4\pi r^2 \tilde{\rho}, \qquad (32)$$

where the corresponding metrics read

$$\frac{d\nu}{dr} = -\frac{2}{\tilde{p} + \tilde{\rho}}\frac{d\tilde{p}}{dr}, \qquad (33)$$

$$e^{-\lambda} \equiv 1 - \frac{2G\tilde{M}}{R}. \qquad (34)$$

Here $\tilde{p}$ and $\tilde{\rho}$ are, respectively, the effective pressure and effective density from Eqs. (7) and (8). To obtain physical results, we use the following mass definition [40]:

$$M \equiv \int 4\pi r^2 \rho dr. \qquad (35)$$

We can obtain radial oscillation equations by disturbing $p(r)$, $\rho(r)$, $\lambda(r)$, and $\nu(r)$ profiles via radial displacement. Then, the perturbation terms are added to the field and the energy-momentum tensor equations. However, we retain only the first term of the corresponding perturbation expansion (standard first-order perturbation approximation). The perturbation terms depend on $e^{i\omega t}$, where ω is the eigenfrequency. The eigenfrequency can be obtained by numerically solving the corresponding radial oscillation equations:

$$\frac{dw}{dr} = -(Q + \omega^2 W)u, \qquad (36)$$

$$\frac{du}{dr} = \frac{w}{P}, \qquad (37)$$

where

$$P = e^{\frac{\lambda + 3\nu}{2}} r^{-2} \tilde{\gamma} \, \tilde{p}, \qquad (38)$$

$$Q = -4e^{\frac{\lambda + 3\nu}{2}} r^{-3}\frac{d\tilde{p}}{dr} - 8\pi G e^{\frac{3\lambda + 3\nu}{2}} r^{-2} \tilde{p}(\tilde{p} + \tilde{\rho}),$$

$$+ e^{\frac{\lambda + 3\nu}{2}} r^{-2} (\tilde{\rho} + \tilde{p})^{-1}\left(\frac{d\tilde{p}}{dr}\right)^2, \qquad (39)$$

$$W = e^{\frac{3\lambda + \nu}{2}} r^{-2}(\tilde{\rho} + \tilde{p}), \qquad (40)$$

$$u = r^2 e^{-\frac{\nu}{2}}\xi. \qquad (41)$$

Here ξ is the Lagrangian radial displacement and $\tilde{\gamma}$ is the effective adiabatic index,

$$\tilde{\gamma} = \left(1 + \frac{\tilde{\rho}}{\tilde{p}}\right)\frac{d\tilde{p}}{d\tilde{\rho}}. \qquad (42)$$

We integrate Eqs. (31) and (32) from the center toward the edge of the star using the Runge-Kutta fourth-order method, with the initial condition at the center is $p(\approx 0) = p_c$. The boundary condition at the edge of the star is $p(R) = 0$, where R is the radius of the star. Equations (33) and (34) are used to calculate the profiles of the metrics. Note that, especially for the metric ν, we require the following boundary condition at the edge:

$$\nu(r \to R) = \ln\left(1 - \frac{2GM}{R}\right). \qquad (43)$$

After obtaining the metrics and other physical quantities such as the mass and distance profiles for a given central pressure p_c, we use the shooting method with an arbitrary trial ω^2 to solve Eqs. (36) and (37). To obtain a unique ω^2, we need a boundary condition where the Lagrangian perturbation for the pressure vanishes at the star's edge. The Lagrangian perturbation for the pressure is given by

$$\Delta p = -e^{-\frac{\lambda}{2} - \nu} w \frac{dp}{d\tilde{p}}. \qquad (44)$$

We also need two corresponding initial conditions, which are derived from $\xi(r \to 0)$ proportional to r. The explicit forms of the initial conditions for w and u are

$$u(r \to 0) = r^3 e^{-\frac{\nu}{2}}, \qquad (45)$$

$$w(r \to 0) = 3\tilde{\gamma} \, \tilde{p} \, e^{\frac{\lambda}{2} + \nu}. \qquad (46)$$

With all of these equations, we can calculate the radial instability of SSs in Rastall gravity theory, just as we might in GR.

The mass-radius relation is an important one: we can directly compare the value obtained from observational data and the one obtained from calculation. Therefore, this relation can be used to study the EoS of neutron stars or SSs. Figures 5 and 6 show the impacts on the SS mass-radius relation of the parameters related to the degree of nonconservative ζ of Rastall gravity: the bag constant B, pairing gap Δ, and strange-quark mass m_s. Note that in our calculations we use the boundary condition $p(R) = 0$ instead of $\tilde{p}(R)$ to obtain an SS radius, and we plot the actual (physical) mass M of the SS instead of the functional mass $\tilde{M}$ [15]. In general, the obtained mass-radius relation results for $\zeta = 0$ show trends similar to those of Lugones and Horvath [41]. By comparing Figs. 5 and 6, it can be understood that, for a fixed SS radius and a fixed m_s, the SS mass also increases with increasing B, and the SS mass decreases with increasing Δ. Meanwhile, for a fixed SS radius, fixed B, and fixed Δ, the SS mass increases with increasing m_s. On the other hand, for fixed m_s, the SS
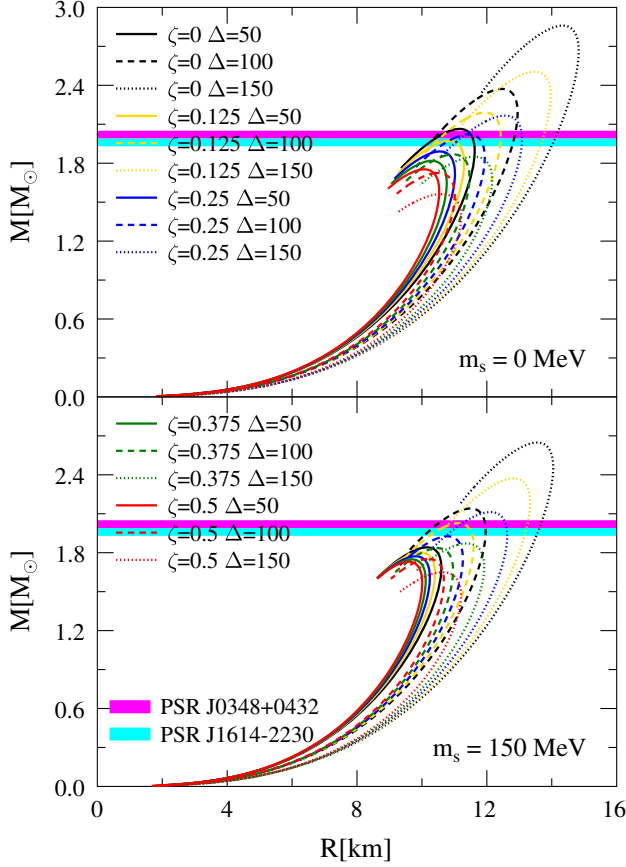
FIG. 5. The total mass M as a function of radius R for $B = 60$ MeV/fm^3 for various values of ζ, m_s, and Δ. Δ has units of MeV. Note that the mass of PSR J1614 − 2230 is taken from Ref. [42], while that of PSR J0348 + 0432 is taken from Ref. [43].
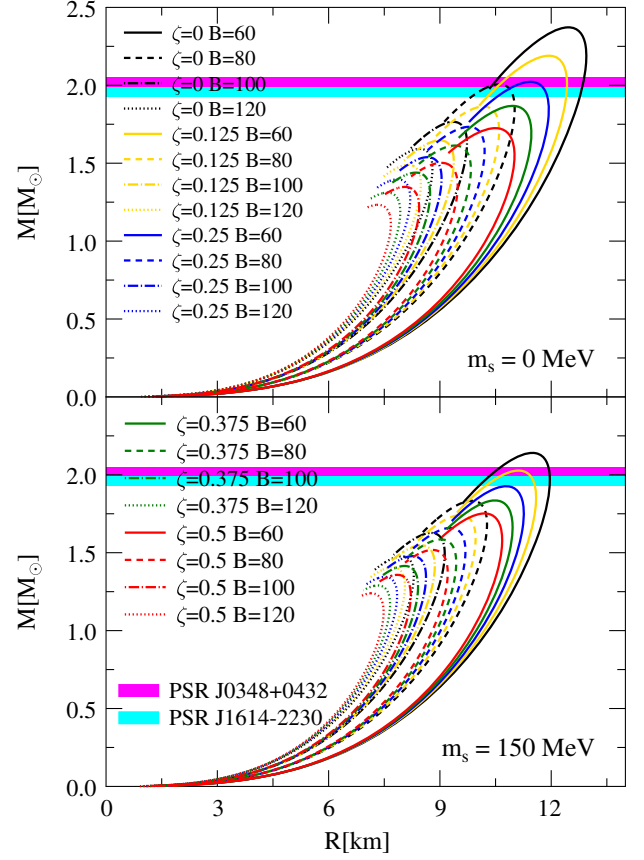

FIG. 6. The total mass M as a function of radius R for $\Delta = 100$ MeV for various values of ζ, m_s, and B. Note that the mass of PSR J1614 − 2230 is taken from Ref. [42], while the one of PSR J0348 + 0432 is taken from Ref. [43].

maximum mass $M_{\max}$ and the associated radius $R_{M_{\max}}$ decrease with increasing B, but the maximum SS mass and the corresponding radius increase with increasing Δ. Similar trends to those in GR are also found for the case of a nonzero ζ value. This similarity is additional evidence that the SS $M_{\max}$ decreases with increasing ζ. This SS mass-radius behavior is a reflection of the SQM EoS discussed in the previous section. This SS mass-radius behavior is also quite different from that found in neutron stars, where the radius but not $M_{\max}$ depends significantly on the ζ value used and on the use of a realistic EoS. Furthermore, previous authors found a conservative bound on the non-GR behavior of Rastall theory which should be at the $\lesssim 1\%$ level [15]. Note that many of the parametrizations used in Figs. 5 and 6 predict maximum masses less than those of the two most recent $M_{\odot}$ constraints [42,43].

To see more clearly the role of ζ in determining the maximum SS mass, we plot $M_{\max}$ as a function of ζ for various values of B, Δ, and m_s (Fig. 7). It is clear that, in general, $M_{\max}$ decreases with increasing ζ, where the decreasing slope of the $M_{\max}$ to ζ relation does not significantly depend on B for the case of $\Delta = m_s = 0$

(MIT bag model). However, this decrease is evidence that the corresponding slope changes with increasing Δ and increasing m_s. However, especially for the nonzero m_s effect, the impact decreases with increasing ζ and the effect becomes insignificant for large values of ζ. Note that if we observe the lowest panel of Fig. 7 for $\Delta = m_s = 0$, $M_{\max}$ still decreases with increasing ζ, even with fixed B.

In a theory with a conserved energy-momentum tensor such as GR, it is known that the point $(M_{\max}, R_{M_{\max}})$ in the SS mass-radius relation coincides with the zero-eigenfrequency mass and radius obtained from radial pulsation analysis $(M_{\omega=0}, R_{\omega=0})$. This correspondence means that $(R_{M_{\max}}, M_{\max})$ is a boundary separating the stable configuration region indicated by $\frac{dM}{d\rho_c} > 0$ from the unstable one indicated by $\frac{dM}{d\rho_c} < 0$. Figure 8 shows that $M_{\max} = M_{\omega=0}$ is still satisfied even if we use the MIT bag model in Rastall gravity theory. The reason is clear: in the MIT bag model, the divergence of the energy-momentum tensor is zero $T^{\mu}_{\nu;\mu} = 0$ due to the role of the specific value of the speed of sound, as discussed in the previous section. It can be seen from Fig. 8 that, for the case $T^{\mu}_{\nu;\mu} \neq 0$, the difference between masses $\Delta M(M_{\max} - M_{\omega=0})$ increases
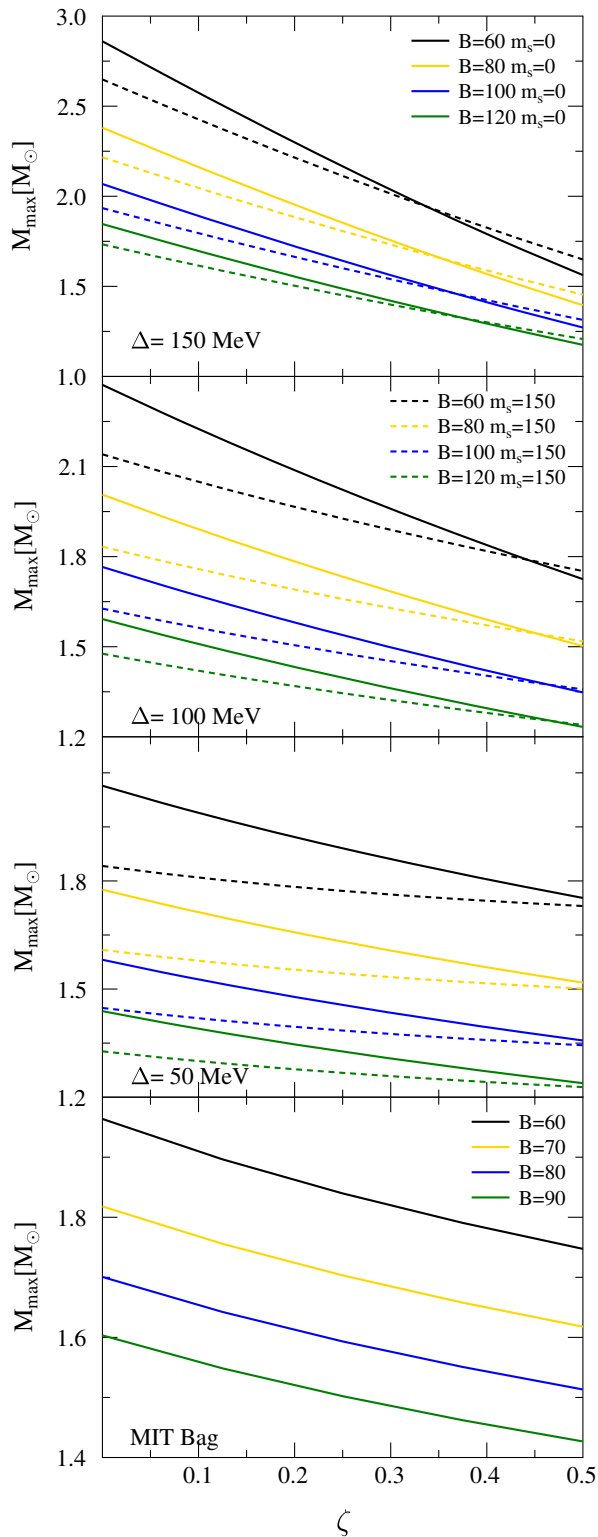
FIG. 7.   The maximum mass as a function of ζ for various values of B, Δ, and m_s.

FIG. 8.   The mass difference between the maximum mass and the mass at which $\omega^2 = 0$, as a function of ζ for various values of B, Δ, and m_s.

with increasing ζ. However, it is interesting to see that ΔM decreases with increasing ζ for large values of ζ if specific conditions are fulfilled such as that shown for the case of $\Delta = 150$ MeV, $m_s = 0$, and $\zeta \geq 0.3$. This behavior
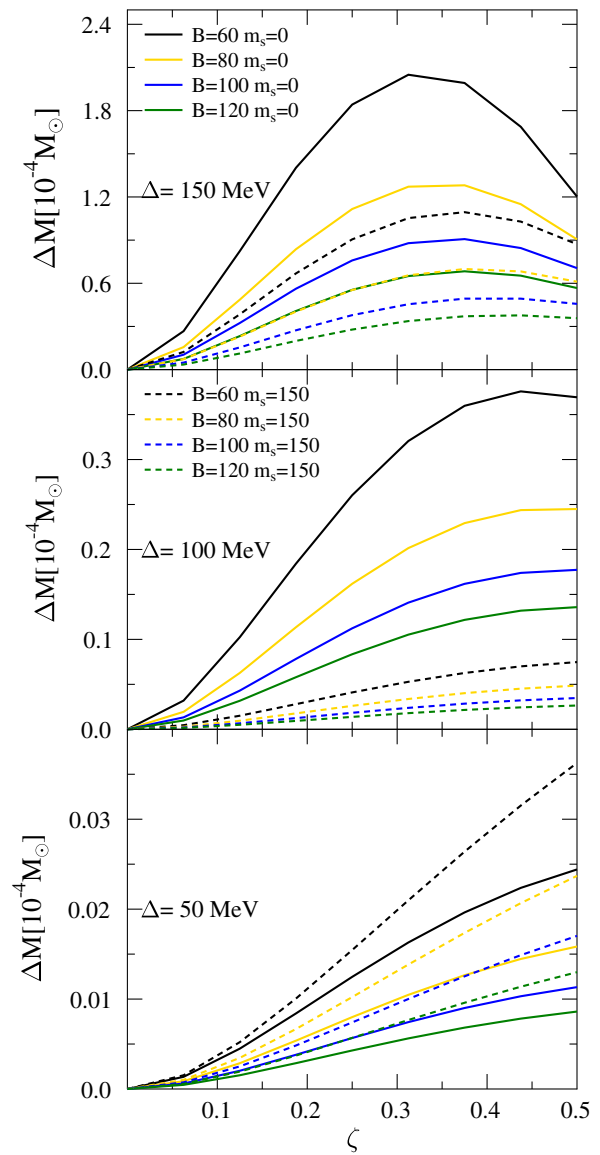
contrasts strongly with what we observe for the other smaller Δ values and $m_s \neq 0$ values: the influence of ζ increases the difference between $M_{\max}$ and $M_{\omega=0}$. We need to emphasize that even though the differences in mass and radius are relatively small (of the order of 10^{-4} $M_\odot$ for the mass and 10^{-3} km for the radius), the differences are not due to numerical artifacts because our code has a numerical precision of around 10^{-13} $M_\odot$ for mass differences and about 10^{-8} km for radius differences. This numerical precision is still smaller than the corresponding mass and radius differences in Figs. 8 and 9. We have checked this for the MIT bag model, where the differences are of the order of our code's numerical precision.

Figure 9 shows additional details regarding the position of the zero-eigenfrequency configuration in the equilibrium.
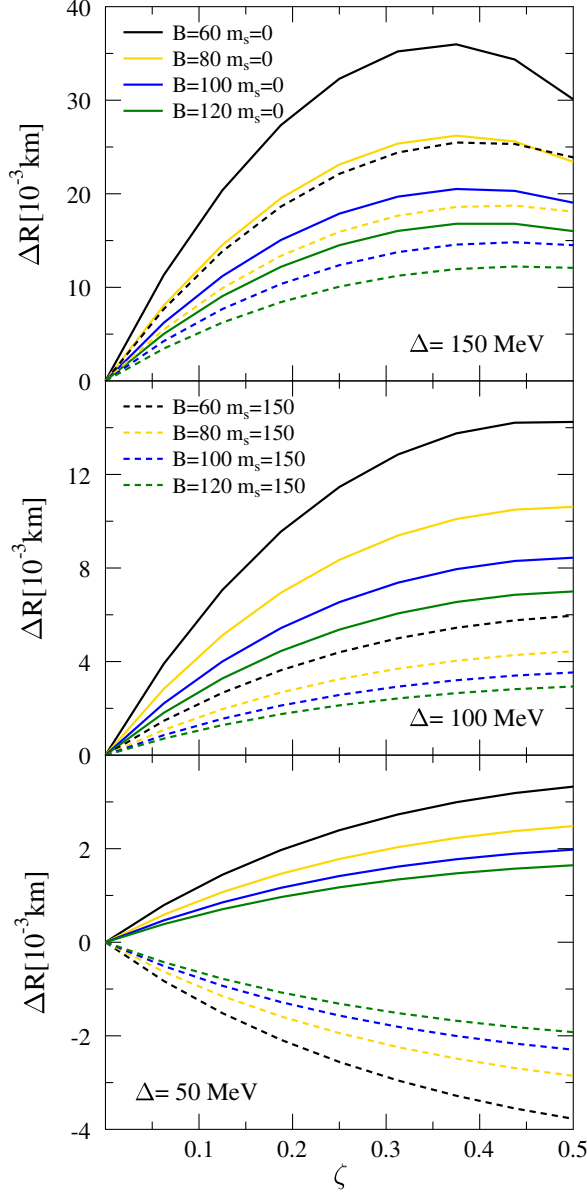
FIG. 9. The radius difference between the model with the maximum mass and the model at which $\omega^2 = 0$, as function of ζ for various values of B, Δ, and m_s.

It is shown that ΔR ($R_{M_{\max}} - R_{\omega=0}$) can be positive or negative depending on the parametrizations. When $\Delta R < 0$, some of the models that verify $dM/d\rho_c > 0$ are unstable because their eigenfrequencies are imaginary. When $\Delta R > 0$ there exist some models verifying $dM/d\rho_c < 0$ that are stable because their eigenfrequencies are real. Thus, it seems that within the Rastall gravity theory, the sign of $dM/d\rho_c$ has no relation with the dynamic stability under small radial perturbations. In most cases, the difference in radii ΔR is positive, indicating that the zero-eigenfrequency mass position lies in the area $\frac{dM}{d\rho_c} < 0$. The case for $\Delta = 150$ MeV and $m_s = 0$ is similar to that in Fig. 8: the difference in radii ΔR is positive but decreases beyond
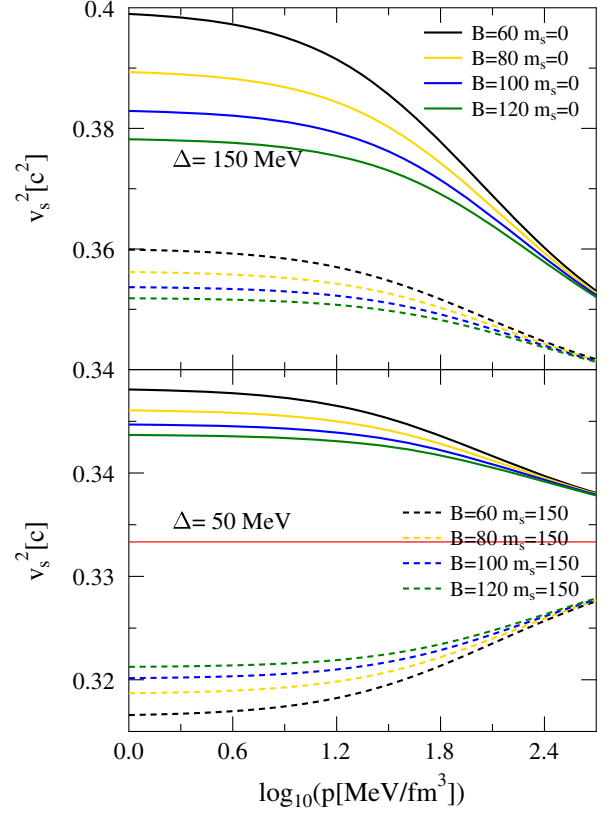

FIG. 10. Pressure versus speed of sound plots for various values of B, Δ, and m_s.

$\zeta \geq 0.3$. We suspect that this behavior is due to the interplay with the stiff EoS of the case with $\Delta = 150$ MeV and $m_s = 0$, which influences the corresponding speed of sound and the effect of a large ζ value. Furthermore, a comparison of the upper and lower panels of Fig. 9 shows that, in the case with $\Delta = 50$ MeV and $m_s = 150$ MeV, ΔR becomes negative, indicating that the zero-eigenfrequency mass position lies in the area $\frac{dM}{d\rho_c} > 0$. From these cases, it is clear that the value of $T^\mu_{\nu;\mu}$ plays a role in changing the stability region. Since $\frac{dp}{dr}$ is negative and ζ is positive, $T^\mu_{\nu;\mu}$ is negative when $\frac{d\rho}{dp} < 3$ or $v_s^2 > 1/3$, but positive when $\frac{d\rho}{dp} > 3$ or $v_s^2 < 1/3$. Figure 10 shows the speed of sound. For the case of $\Delta = 50$ (lower panel), the behavior v_s^2 changes if we change m_s. It is clear that this change makes $T^\mu_{\nu;\mu} < 0$ for $m_s = 0$ MeV but makes $T^\mu_{\nu;\mu} > 0$ for $m_s = 150$ MeV. We conclude that $T^\mu_{\nu;\mu} < 0$ will shift the stability boundary towards the area $\frac{dM}{d\rho_c} < 0$ and $T^\mu_{\nu;\mu} > 0$ will shift the stability boundary toward the area $\frac{dM}{d\rho_c} > 0$. This behavior is due to the Rastall nonconservation term increasing the SQM pressure to support the SS against gravitational collapse. Arbañil and Malheiro [27,44] studied the radial oscillations of SS anisotropy and SS charge. They also found that the stability boundary shifted from $\frac{dM}{d\rho_c} = 0$ in both cases, where an increase in the anisotropic free parameter or in the SS

charge causes the stability boundary to shift to the $\frac{dM}{d\rho_c} < 0$ region. On the other hand, a decrease in the anisotropic free parameter or in the SS charge causes the stability boundary to shift to the $\frac{dM}{d\rho_c} > 0$ region. Thus, the anisotropic free parameter and SS charge play roles similar to the Rastall nonconservation parameter ζ (especially for matter with $v_s^2 > 1/3$) in supporting the pressure of the corresponding matter against gravitational collapse. The reverse applies for matter with $v_s^2 < 1/3$. We also note that a similar effect is also found in models of hybrid stars where chemical reactions at the quark-hadron interface are much slower than the oscillation time scale (see Refs. [45,46]).

V. CONCLUSIONS

In this work, we used ideal fluid energy conditions to determine the allowed ζ range and thereby constrained the Rastall free parameter η. We studied the SS mass-radius relation and determined the corresponding stability using the MIT bag model for SQM with a CFL state in Rastall gravity theory. We found that corresponding energy conditions constrain the Rastall free parameter η to a rather wide range: $\eta \geq 1$ and $\eta \leq 0$. However, if this parameter range is translated to the range of the ζ parameter, we can obtain a finite, narrow range: $0 \leq \zeta \leq 0.5$. The physical interpretation of ζ is more direct than that of η. The free parameter ζ can be assumed to influence the nonconservation of the energy-momentum tensor. $\zeta = 0$ indicates that the energy-momentum tensor is conserved, whereas $\zeta = 0.5$ indicates the maximal deviation allowed by energy conditions for energy-momentum nonconservation. However, ζ is not the only variable influencing energy-momentum nonconservation: the gradient of the scalar energy-momentum tensor T also plays a crucial role in the nonconservation of the energy-momentum tensor. In

Rastall gravity theory, the energy-momentum tensor is still conserved when $\frac{dT}{dr} = 0$, even though the parameter $\zeta \neq 0$. The MIT bag model with a constant speed of sound such as $v_s = \frac{1}{\sqrt{3}}$ is one such example. We also found that, for SQM based on the MIT bag model with a CFL state in Rastall gravity theory, the mass-radius relation of SSs depends on the interplay of m_s, B, Δ, and ζ. In general, for a fixed radius and m_s and independent of ζ, the SS mass increases with increasing B, and decreases with increasing Δ. Meanwhile, for fixed radius, B, and Δ, the SS mass increases with increasing m_s. On the other hand, for fixed m_s, the SS maximum mass $M_{\max}$ and the associated radius $R_{M_{\max}}$ decrease with increasing B, but $M_{\max}$ and $R_{M_{\max}}$ increase with increasing B. This behavior is also evidence that the SS $M_{\max}$ decreases with increasing ζ. We also found that the stability of SSs with respect to radial oscillation perturbations in Rastall gravity theory is rather different than that in GR because of the impact of the nonconservation of the energy-momentum tensor. If $T_{\nu;\mu}^{\mu} \neq 0$, the inequality $\frac{dM}{d\rho_c}$ becomes a necessary condition, but it is not sufficient for recognizing stable configurations. If $T_{\nu;\mu}^{\mu} < 0$ and $T_{\nu;\mu}^{\mu} > 0$, the stability boundary position determined from the SQM zero mode of radial oscillation perturbations shifts to the areas with $\frac{dM}{d\rho_c} < 0$ and $\frac{dM}{d\rho_c} > 0$, respectively. This shift occurs because the Rastall nonconservation term increases the pressure on the SQM, supporting the SS against collapse, especially in situations with $v_s^2 > 1/3$.

[1] E. Berti *et al.*, Classical Quantum Gravity **32**, 243001 (2015).
[2] D. Psaltis, Living Rev. Relativity **11**, 9 (2008).
[3] T. Clifton, P. G. Ferreira, A. Padilla, and C. Skordis, Phys. Rep. **513**, 1 (2012).
[4] P. Rastall, Phys. Rev. D **6**, 3357 (1972).
[5] T. Koivisto, Classical Quantum Gravity **23**, 4289 (2006).
[6] T. Harko, F. S. N. Lobo, S. Nojiri, and S. D. Odintsov, Phys. Rev. D **84**, 024020 (2011).
[7] O. Minazzoli, Phys. Rev. D **88**, 027506 (2013).
[8] R. V. d. Santos and J. A. Nogales, arXiv:1701.08203.
[9] Ö. Akarsu, J. D. Barrow, S. Çikintoğlu, K. Y. Ekşi, and N. Katirci, Phys. Rev. D **97**, 124017 (2018).
[10] G. A. Carvalho, P. H. R. S. Moraes, I. dos Santos, Jr., B. S. Goncalves, and M. Malheiro, arXiv:1904.00282.
[11] S. Calogero and H. Velten, J. Cosmol. Astropart. Phys. 11 (2013) 025.
[12] H. Moradpour, Y. Heydarzade, F. Darabi, and I. G. Salako, Eur. Phys. J. C **77**, 259 (2017).
[13] V. Dzhunushaliev and H. Quevedo, Gravitation Cosmol. **23**, 280 (2017).
[14] T. Josset, A. Perez, and D. Sudarsky, Phys. Rev. Lett. **118**, 021102 (2017).
[15] A. M. Oliveira, H. E. S. Velten, J. C. Fabris, and L. Casarini, Phys. Rev. D **92**, 044020 (2015).
[16] M. Visser, Phys. Lett. B **782**, 83 (2018).
[17] F. Darabi, H. Moradpour, I. Licata, Y. Heydarzade, and C. Corda, Eur. Phys. J. C **78**, 25 (2018).
[18] S. Hansraj, A. Banerjee, and P. Channuie, Ann. Phys. (Amsterdam) **400**, 320 (2019).

[19] G. Lugones and J. E. Horvath, Phys. Rev. D **66**, 074017 (2002).

[20] L. Paulucci and J. E. Horvath, Phys. Rev. C **78**, 064907 (2008).

[21] M. G. Alford, A. Schmitt, K. Rajagopal, and T. Schäfer, Rev. Mod. Phys. **80**, 1455 (2008).

[22] M. G. Alford and K. Schwenzer, Phys. Rev. Lett. **113**, 251102 (2014).

[23] M. Alford, K. Rajagopal, S. Reddy, and F. Wilczek, Phys. Rev. D **64**, 074017 (2001).

[24] S. Chandrasekhar, Phys. Rev. Lett. **12**, 114 (1964).

[25] A. Brillante and I. N. Mishustin, Europhys. Lett. **105**, 39001 (2014).

[26] C. Vasquez Flores and G. Lugones, Phys. Rev. D **82**, 063006 (2010).

[27] J. D. V. Arbañil and M. Malhairo, J. Cosmol. Astropart. Phys. 11 (2016) 012.

[28] G. Panotopoulos and I. Lopes, Phys. Rev. D **98**, 083001 (2018).

[29] L. L. Smalley, Nuovo Cimento B **80**, 42 (1984).

[30] S. Capozziello, F. S. Lobo, and J. P. Mimoso, Phys. Lett. B **730**, 280 (2014).

[31] K. Atazadeh and F. Darabi, Gen. Relativ. Gravit. **46**, 1664 (2014).

[32] J. Santos, J. S. Alcaniz, M. J. Reboucas, and F. C. Carvalho, Phys. Rev. D **76**, 083513 (2007).

[33] H. Moradpour and I. G. Salako, Adv. High Energy Phys. (Hindawi) **2016**, 1 (2016).

[34] C. E. M. Batista, M. H. Daouda, J. C. Fabris, O. F. Piattella, and D. C. Rodrigues, Phys. Rev. D **85**, 084008 (2012).

[35] C. E. M. Batista, J. C. Fabris, O. F. Piattella, and A. Velasquez-Toribio, Eur. Phys. J. C **73**, 2425 (2013).

[36] A. M. Oliveira, H. E. S. Velten, and J. C. Fabris, Phys. Rev. D **93**, 124020 (2016).

[37] M. Daouda, J. C. Fabris, A. Oliveira, F. Smirnov, and H. Velten, arXiv:1701.08203.

[38] C. V. Flores and G. Lugones, Phys. Rev. C **95**, 025808 (2017).

[39] E. Farhi and R. L. Jaffe, Phys. Rev. D **30**, 2379 (1984).

[40] H. Velten, A. M. Oliveira, and A. Wojnar, Proc. Sci., MPCS2015 (**2016**) 025 [arXiv:1601.03000].

[41] G. Lugones and J. E. Horvath, Astron. Astrophys. **403**, 173 (2003).

[42] P. B. Demorest, T. Pennucci, S. M. Ransom, M. S. E. Roberts, and J. W. T. Hessels, Nature (London) **467**, 1081 (2010); see also related recent report in Z. Arzoumanian *et al.*, Astrophys. J. Suppl. Ser. **235**, 37 (2018).

[43] J. Antoniadis *et al.*, Science **340**, 1233232 (2013).

[44] J. D. V. Arbañil and M. Malheiro, Phys. Rev. D **92**, 084009 (2015).

[45] J. P. Pereira, C. V. Flores, and G. Lugones, Astrophys. J. **860**, 12 (2018).

[46] M. Mariani, M. G. Orsaria, I. F. Ranea-Sandova, and G. Lugones, Mon. Not. R. Astron. Soc. **489**, 4261 (2019).